MNRAS **000**, 1–15 (2015) Preprint 15 December 2015 Compiled using MNRAS LATEX style file v3.0

Measurement of the dipole in the cross-correlation function of galaxies

Enrique Gaztanaga[1⋆], Camille Bonvin[2†], Lam Hui[3‡]
[1] *Institut de Ciències de l'Espai (IEEC-CSIC), 08193 Bellaterra, Barcelona, Spain*
[2] *CERN, Theory Division, 1211 Geneva 23, Switzerland*
[3] *Institute for Strings, Cosmology and Astroparticle Physics and Department of Physics, Columbia University, New York 10027, U.S.A.*

arXiv:1512.03918v1 [astro-ph.CO] 12 Dec 2015

Accepted XXX. Received YYY; in original form ZZZ

ABSTRACT

It is usually assumed that in the linear regime the two-point correlation function of galaxies contains only a monopole, quadrupole and hexadecapole. Looking at cross-correlations between different populations of galaxies, this turns out not to be the case. In particular, the cross-correlations between a bright and a faint population of galaxies contain also a dipole. In this paper we present the first measurement of this dipole. We discuss the three types of effects that contribute to the dipole: relativistic distortions, evolution effects and wide-angle effects. We show that the relativistic distortions and the evolution effects are too small to be detected in the LOWz and CMASS sample of the BOSS survey. We discuss the convention-dependent nature of the wide-angle effect and we show that with the appropriate choice of kernel, a particular version of the wide-angle effect (that we call large-angle effect) can be significantly enhanced. We measure this effect in the dipole with a signal-to-noise of 50, which is as good as the one of the monopole. We emphasise that the large-angle dipole does not contain new statistical information, since it is just a geometrical combination of the monopole and the quadrupole. However it is conceivable that it is sensitive to different systematics.

Key words: Large-scale structure of Universe – cross-correlation functions – wide-angle effects

1 INTRODUCTION

The two-point correlation function of galaxies is a powerful cosmological probe. It has been measured with increasing precision in various surveys over the last 50 years. In those measurements, the correlation function is implicitly assumed to be symmetric under the exchange of the galaxies in the pair $\langle\Delta(\mathbf{x}_i)\Delta(\mathbf{x}_j)\rangle = \langle\Delta(\mathbf{x}_j)\Delta(\mathbf{x}_i)\rangle$, where $\Delta(\mathbf{x}_i)$ represents the fractional over-density of galaxies in pixel i. In redshift-space, the correlation function can be expressed as a function of the pixels separation d_{ij}, the redshift of the pair, and the angle that the pair makes with the observer's line-of-sight γ_{ij}. The symmetry of the correlation function implies that it depends only on even powers of $\cos\gamma_{ij}$. More precisely, in the distant-observer approximation, the two-point correlation function can simply be written as the sum of a monopole, a quadrupole and an hexadecapole (Kaiser 1987; Lilje & Efstathiou 1989; Hamilton 1992). The measurement of these multipoles constitutes one of the great success of large-scale structure surveys since it provides a direct measurement of the growth rate of cosmological perturbations f (see e.g. Hawkins et al. 2003; Zehavi et al. 2005; Guzzo et al. 2008; Cabre & Gaztanaga 2009; Song et al. 2011; Samushia et al. 2014).

Recently it has been shown that if one splits the galaxies into different populations (with e.g. different luminosities or colours), the form of the two-point correlation function becomes more complex. In particular, the cross-correlations between a bright and a faint population of galaxies acquire an anti-symmetric part (McDonald 2009; Yoo et al. 2012; Croft 2013; Bonvin et al. 2014): $\langle\Delta_{\rm B}(\mathbf{x}_i)\Delta_{\rm F}(\mathbf{x}_j)\rangle \neq \langle\Delta_{\rm F}(\mathbf{x}_i)\Delta_{\rm B}(\mathbf{x}_j)\rangle$. The goal of this paper is to measure, for the first time, this anti-symmetric part in the correlation function.

As shown in Bonvin et al. (2014); Bonvin (2014), there are three types of effects that generate an anti-symmetry in the correlation function [1]. The first contribution is due to *relativistic distortions* in the number count of galaxies Δ.

⋆ gazta@ice.cat
† camille.bonvin@cern.ch
‡ lhui@astro.columbia.edu

[1] Note that here we do not consider possible primordial anti-

© 2015 The Authors

This observable is indeed not only affected by density fluctuations and by the gradient of the velocity, as assumed in the standard redshift-space distortion expression, but also by various contributions of the gravitational potentials and of the peculiar velocity (Yoo et al. 2009; Yoo 2010; Bonvin & Durrer 2011; Challinor & Lewis 2011; Jeong et al. 2012). Among all these effects, one can show that the following combination of gravitational redshift and Doppler terms generates an anti-symmetry in the correlation function

$$\Delta^{\rm anti}(\mathbf{x},z) = \frac{1}{\mathcal{H}}\partial_r\Psi + \frac{1}{\mathcal{H}}\dot{\mathbf{V}}\cdot\mathbf{n} + \left[1 - \frac{\dot{\mathcal{H}}}{\mathcal{H}^2} - \frac{2}{r\mathcal{H}} + 5s\left(1-\frac{1}{r\mathcal{H}}\right)\right]\mathbf{V}\cdot\mathbf{n}\,, \quad (1)$$

where Ψ is the time-component of the metric [2], $\mathbf{V}$ is the peculiar velocity, $\mathbf{n}$ is the observed direction, $\mathcal{H}$ is the conformal Hubble parameter, r is the conformal distance to the source and s is the slope of the luminosity function. A dot denotes derivative with respect to conformal time η. The terms in eq. (1) contain all one gradient of the potential, which is responsible for the anti-symmetry [3]. Note that in Fourier space, these terms have the particularity to generate an imaginary part to the power spectrum (McDonald 2009; Yoo et al. 2012).

The second source of anti-symmetry in the correlation function comes from the *evolution* of the bias and of the growth rate. This evolution –which differs for different populations of galaxies– generates a systematic asymmetry between e.g. the number of faint galaxies in front and behind a bright galaxy.

Finally, the third effect generating an anti-symmetry in the two-point function is the *wide-angle* effect. Beyond the distant-observer approximation, the line-of-sight to the two galaxies in the pair are not parallel. This generates corrections to the standard Kaiser expression for the monopole, quadrupole and hexadecapole (see e.g. Hamilton 1997; Szalay et al. 1998; Szapudi 2004; Papai & Szapudi 2008; Raccanelli et al. 2010; Samushia et al. 2012; Montanari & Durrer 2012; Bertacca et al. 2012; Yoo & Seljak 2015; Reimberg et al. 2015), but it also induces an additional anti-symmetric contribution to the two-point correlation function (Bonvin et al. 2014). The name *wide-angle effect* has been used to denote different things in the literature. Some authors (e.g. Reimberg et al. 2015) call wide-angle effect all contributions to the multipoles that are suppressed by one or more powers of d/r where d is the comoving separation between galaxies and r is the comoving distance to the pair. For other authors (e.g. Hamilton 1997; Raccanelli et al. 2010) the wide-angle effect refers to the fact that at large separation the two-point function in redshift-space depends not only on the separation between galaxies d and on the orientation of the pair with respect to the observer, but also on a third variable encoding the difference between the line-of-sight to each of the galaxies. In the following we adopt this second terminology: we reserve the name wide-angle effect for the intrinsic anti-symmetry generated by the fact that redshift-space distortions depend on *two* line-of-sights, and we call *large-angle* effect the other terms suppressed by powers of d/r (see 2.2 for more detail).

The anti-symmetry generated by the relativistic, evolution, wide-angle and large-angle effects can be expanded in odd multipoles of $\cos\gamma_{ij}$ (Bonvin et al. 2014; Raccanelli et al. 2014). The dominant contribution is a dipole, simply proportional to $\cos\gamma_{ij}$. In this paper, we show how to measure this dipole in the two-point correlation function of galaxies. Note that this dipole is completely different from the kinematic dipole due to our motion with respect to the frame of the Cosmic Microwave Background (Kogut et al. 1993). The kinematic dipole is a dipole around the observer, whereas the dipole we are measuring in this paper is a dipole around each of the bright galaxies in the survey.

The remainder of the paper is organised as follow: in section 2 we present the method used to extract the dipole from the two-point correlation function of galaxies. We show that depending on the choice of kernel, we are sensitive to different combinations of terms. In section 3 we apply our method to the BOSS LOWz and CMASS samples. We show that the contributions due to the relativistic distortions, evolution and wide-angle effect are too small to be detected in these samples. We calculate the signal-to-noise of these contributions and show that it is of the order of 0.2. On the other hand, we show that an appropriate choice of kernel allows us to measure the large-angle effect and to separate it from the relativistic, evolution and wide-angle contributions. We detect this large-angle dipole with a signal-to-noise of 50. This corresponds to the first detection of the large-angle effect in large-scale structure surveys. As explained in section 3.3, to detect the large-angle effect with such a large signal-to-noise we must construct an estimator which exactly vanishes in the distant-observer approximation. This allows us to isolate the large-angle effect from the relativistic, evolution and wide-angle contributions, but also to remove the flat-sky part of the noise, i.e. the noise due to Newtonian effects. In section 3.4, we compare our method with the estimator $z_{\rm shell}$ presented in Croft (2013) and show that a simple expression relates the two estimators. Note that in this paper we are interested in galaxy correlations at large scales. We work therefore in linear perturbation theory, where the non-linear effects described in Zhao et al. (2013); Kaiser (2013) are negligible. Finally in section 3.5 we show that the large-angle dipole can also be measured with a single population of galaxies if we choose the appropriate kernel. We conclude in section 4.

2 EXTRACTING THE DIPOLE

As mentioned above, to measure an anti-symmetry in the two-point correlation function we need in general more than one population of galaxies. In the following, we split therefore the galaxies into a bright population and a faint population based on their luminosity. In a companion paper (Bonvin et al. 2015), we consider the more general case of multiple populations of galaxies with different luminosities and we

symmetries in the correlation function generated for example by a primordial vector field (Dai et al. 2015).

[2] We use here the following convention for the metric $ds^2 = a^2\left[-(1+2\Psi)d\eta^2 + (1-2\Phi)\delta_{ij}dx^i dx^j\right]$, where a is the scale factor and η denotes conformal time.

[3] Gravitational lensing also generates an anti-symmetry in the two-point function. However, as shown in Bonvin et al. (2014) this contribution is always significantly smaller than the terms in eq. (1) and it can safely be neglected.

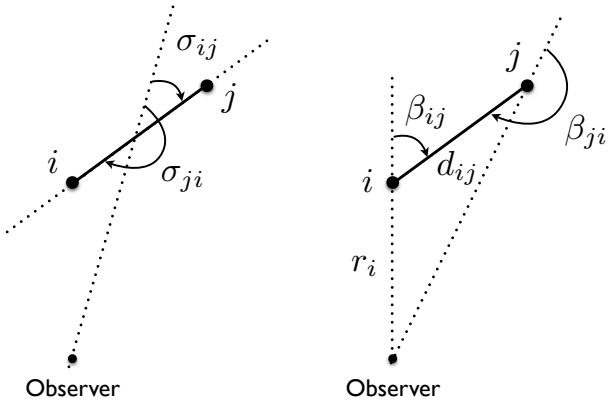

Figure 1. Representation of the two cases we consider for the line-of-sight angle: σ_{ij} (left panel) and β_{ij} (right panel). In section 3, we measure the dipole with $\mu_{12} \equiv \cos\sigma_{ij}$ and with $\mu_1 = \cos\beta_{ij}$. We also construct an estimator based on the difference between the two angles: $\cos\beta_{ij} - \cos\sigma_{ij}$.

show how the dipole can be optimally extracted in this case. Here we restrict ourselves to two populations and we adjust the threshold between the bright and the faint population to obtain a similar number of galaxies in each sample.

For each pixel i in the sky, we count the number of bright galaxies $n_{\rm B}(\mathbf{x}_i)$ and the number of faint galaxies $n_{\rm F}(\mathbf{x}_i)$. We construct the over-density of galaxies

$$\delta n_{\rm B}(\mathbf{x}_i) = n_{\rm B}(\mathbf{x}_i) - d\bar{n}_{\rm B} \quad \text{and} \quad \delta n_{\rm F}(\mathbf{x}_i) = n_{\rm F}(\mathbf{x}_i) - d\bar{n}_{\rm F}\,, \tag{2}$$

where $d\bar{n}_{\rm B}$ and $d\bar{n}_{\rm F}$ denote the mean number of galaxies per pixel. Note that these quantities depend on the size of the pixels. We combine the two populations of galaxies with a kernel $w_{\mathbf{x}_i\mathbf{x}_j L_i L_j}$ designed to extract the dipole

$$\hat{\xi} = \sum_{ij} \sum_{L_i L_j = {\rm B,F}} w_{\mathbf{x}_i\mathbf{x}_j L_i L_j}\, \delta n_{L_i}(\mathbf{x}_i)\delta n_{L_j}(\mathbf{x}_j)\,. \tag{3}$$

To isolate the dipole from the other multipoles, the kernel $w_{\mathbf{x}_i\mathbf{x}_j L_i L_j}$ must be proportional to the cosine of the angle γ_{ij} that the pair of pixels makes with the line-of-sight. It must also depend on the respective luminosities of the pixels, L_i and L_j. A simple way of constructing a kernel with these properties is

$$w_{\mathbf{x}_i\mathbf{x}_j L_i L_j} = a_N \cos\gamma_{ij L_i L_j}\, \delta_K(d_{ij} - d)\,, \tag{4}$$

where

$$\gamma_{ij L_i L_j} = \begin{cases} \gamma_{ij} & \text{if} \quad L_i > L_j\,, \\ \gamma_{ji} & \text{if} \quad L_i < L_j\,. \end{cases} \tag{5}$$

Here a_N is a normalisation factor (which depends on the pair separation $d = d_{ij}$)

$$a_N = \frac{3}{8\pi}\left(N_{\rm tot}\ell_p d^2 \bar{N}\bar{n}_{\rm B}\bar{n}_{\rm F}\right)^{-1}, \tag{6}$$

with $N_{\rm tot}$ the total number of galaxies, ℓ_p the length of a cubic pixel, $\bar{N}$ the mean number density of galaxies, and $\bar{n}_{\rm B}$ and $\bar{n}_{\rm F}$ the fractional number of bright and faint galaxies. Note that this kernel is slightly different from the one chosen in Bonvin et al. (2015), which we discuss in appendix A.

Beyond the distant-observer approximation, there are different ways of choosing the angle between the pair of galaxies and the observer's line-of-sight. In figure 1 we show two possible choices: $\gamma_{ij} = \sigma_{ij}$, i.e. the angle between the median and the vector connecting the median to j; and $\gamma_{ij} = \beta_{ij}$, i.e. the angle between the direction of the pixel i and the vector connecting i to j.

2.1 Relativistic and evolution dipole

The relativistic dipole and the dipole due to evolution are insensitive to the choice of angle [4]. In the continuous limit the mean of these contributions can be written as (see Bonvin et al. 2014, for more detail)

$$\langle\hat{\xi}^{\rm rel}\rangle = (b_{\rm B} - b_{\rm F})\left(\frac{\dot{\mathcal{H}}}{\mathcal{H}^2} + \frac{2}{r\mathcal{H}}\right)\frac{\mathcal{H}}{\mathcal{H}_0}\frac{f}{2\pi^2} \times \int dk k \mathcal{H}_0 P(k,\bar{z}) j_1(kd)\,, \tag{7}$$

$$\langle\hat{\xi}^{\rm evol}\rangle = \frac{d}{r}\left\{\frac{r}{6}\Big[(b_{\rm B} - b_{\rm F})f' - f(b'_{\rm B} - b'_{\rm F})\Big]\left(C_0(d) - \frac{4}{5}C_2(d)\right) + \frac{r}{2}(b_{\rm B}b'_{\rm F} - b'_{\rm B}b_{\rm F})C_0(d)\right\}, \tag{8}$$

where $P(k,\bar{z})$ is the density power spectrum at the mean redshift of the survey:

$$\langle\delta(\mathbf{k},\bar{z})\delta(\mathbf{k}',\bar{z})\rangle = (2\pi)^3 P(k,\bar{z})\delta_D(\mathbf{k}+\mathbf{k}')\,, \tag{9}$$

and

$$C_\ell(d) = \frac{1}{2\pi^2}\int dk k^2 P(k,\bar{z}) j_\ell(kd)\,, \quad \ell = 0, 2\,. \tag{10}$$

Note that contrary to the angular power spectrum, which is very sensitive to the size of the redshift bin within which the pairs of pixels i, j are averaged (Bonvin & Durrer 2011; Di Dio et al. 2014), the two-point correlation function $\hat{\xi}$ is almost insensitive to the binning procedure (Bonvin 2014). Therefore in eqs. (7) and (8) we approximate the average over redshift by the value of the correlation function at the mean redshift of the survey $\bar{z}$.

2.2 Wide-angle and large-angle dipole

Contrary to the relativistic and evolution dipole, the wide-angle and large-angle dipole depend strongly on the choice of angle (note that this dependence is discussed in detail in Reimberg et al. (2015) for the case of one population of galaxies). Using the median angle σ_{ij}, we find for the mean of the wide-angle effect

$$\langle\hat{\xi}^{{\rm wide}\,\sigma}\rangle = a_N d\bar{n}_{\rm B} d\bar{n}_{\rm F} \sum_{ij} \cos\sigma_{ij}\,\delta_K(d_{ij} - d) \times \Big[\langle\Delta_{\rm B}(\mathbf{x}_i)\Delta_{\rm F}(\mathbf{x}_j)\rangle - \langle\Delta_{\rm B}(\mathbf{x}_j)\Delta_{\rm F}(\mathbf{x}_i)\rangle\Big]^{\rm wide}\,, \tag{11}$$

where we have used that $\cos\sigma_{ji} = -\cos\sigma_{ij}$ (see figure 1). In Bonvin et al. (2014) we calculated the term in bracket

[4] This is correct at lowest order in d/r. At large separation, both the relativistic dipole and the dipole due to evolution receive corrections of the order $(d/r)^2$. The specific form of these corrections depend on the choice of angle. For the scales we are interested in however, these differences are completely negligible.

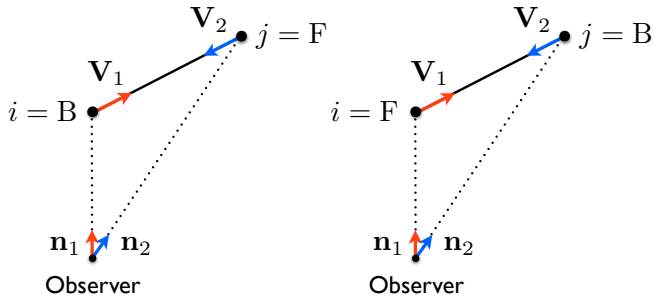

Figure 2. Contribution to the wide-angle dipole (12) from the correlation between density and redshift-space distortion. In the flat-sky we have $\mathbf{n}_1 = \mathbf{n}_2 = \mathbf{n}$ so that $|\mathbf{V}_1 \cdot \mathbf{n}| = |\mathbf{V}_2 \cdot \mathbf{n}|$ and the contributions from the left and right panels cancel. In the full sky however $\mathbf{n}_1 \neq \mathbf{n}_2$ and the two panels combine to give (12).

as a function of the angle β_{ij}. Here we need to rewrite it in terms of σ_{ij}. The calculation is presented in appendix B. We find in the continuous limit

$$\langle\hat{\xi}^{\mathrm{wide}\,\sigma}\rangle = \frac{2f}{5}(b_{\mathrm{B}} - b_{\mathrm{F}})\frac{d}{r}C_2(d)\,. \tag{12}$$

The physical origin of this wide-angle effect can be understood by looking at figure 2. From the left panel, we see that the correlation between redshift-space distortion and density generates a contribution proportional to $|\mathbf{V}_1 \cdot \mathbf{n}_1|$ weighted by the bias of the faint galaxy plus a contribution proportional to $|\mathbf{V}_2 \cdot \mathbf{n}_2|$ weighted by the bias of the bright galaxy. To these contributions we must, according to eq. (11), subtract the contributions from the right panel of figure 2. In this case, the contribution proportional to $|\mathbf{V}_1 \cdot \mathbf{n}_1|$ is weighted by the bias of the bright galaxy and the contribution proportional to $|\mathbf{V}_2 \cdot \mathbf{n}_2|$ is weighted by the bias of the faint galaxy. In the distant-observer approximation we have $\mathbf{n}_1 = \mathbf{n}_2 = \mathbf{n}$. Since on average the galaxies tend to attract each other, we have then $|\mathbf{V}_1 \cdot \mathbf{n}| = |\mathbf{V}_2 \cdot \mathbf{n}|$ so that the contributions from the left and right panels of figure 2 cancel. At large scale however, when the distant-observer approximation breaks down $\mathbf{n}_1 \neq \mathbf{n}_2$. The contributions from the right and left panels of figure 2 are not exactly the same and they give rise to eq. (12).

If instead of using σ_{ij} to measure the dipole we use β_{ij} we obtain

$$\langle\hat{\xi}^{\mathrm{wide}\,\beta}\rangle = a_N d\bar{n}_{\mathrm{B}} d\bar{n}_{\mathrm{F}} \sum_{ij} \Big[\langle\Delta_{\mathrm{B}}(\mathbf{x}_i)\Delta_{\mathrm{F}}(\mathbf{x}_j)\rangle \cos\beta_{ij} + \langle\Delta_{\mathrm{B}}(\mathbf{x}_j)\Delta_{\mathrm{F}}(\mathbf{x}_i)\rangle \cos\beta_{ji}\Big]^{\mathrm{wide}} \delta_K(d_{ij} - d)\,. \tag{13}$$

From figure 1 we see that at large separation $\cos\beta_{ij} \neq -\cos\beta_{ji}$. In the full sky we have

$$\cos\beta_{ji} = -\frac{r_i\cos\beta_{ij} + d_{ij}}{\sqrt{r_i^2 + 2r_i d_{ij}\cos\beta_{ij} + d_{ij}^2}} = -\cos\beta_{ij} - \frac{d_{ij}}{r_i}\left(1 - \cos^2\beta_{ij}\right) + \mathcal{O}\left(\frac{d_{ij}}{r_i}\right)^2 . \tag{14}$$

Inserting this into eq. (13) we obtain at lowest order in d_{ij}/r_i

$$\langle\hat{\xi}^{\mathrm{wide}\,\beta}\rangle = a_N d\bar{n}_{\mathrm{B}} d\bar{n}_{\mathrm{F}} \times \sum_{ij}\Bigg\{\Big[\langle\Delta_{\mathrm{B}}(\mathbf{x}_i)\Delta_{\mathrm{F}}(\mathbf{x}_j)\rangle - \langle\Delta_{\mathrm{B}}(\mathbf{x}_j)\Delta_{\mathrm{F}}(\mathbf{x}_i)\rangle\Big]^{\mathrm{wide}}\cos\beta_{ij} - \langle\Delta_{\mathrm{B}}(\mathbf{x}_j)\Delta_{\mathrm{F}}(\mathbf{x}_i)\rangle\frac{d_{ij}}{r_i}\left(1 - \cos^2\beta_{ij}\right)\Bigg\}\delta_K(d_{ij} - d)\,. \tag{15}$$

The term in the second line gives rise to eq. (12) (since the bracket is already of order d_{ij}/r, we can replace β_{ij} by σ_{ij} in the second line). The term in the third line however is a novel contribution, specific to this particular choice of angle. To differentiate this contribution from the one in eq. (12) we call it the *large-angle* contribution [5]. In the continuous limit, we obtain

$$\langle\hat{\xi}^{\mathrm{wide}\,\beta}\rangle = \langle\hat{\xi}^{\mathrm{wide}\,\sigma}\rangle + \langle\hat{\xi}^{\mathrm{large}}\rangle\,, \tag{16}$$

where

$$\langle\hat{\xi}^{\mathrm{large}}\rangle = \frac{d}{r}\Bigg\{\left[b_{\mathrm{B}}b_{\mathrm{F}} + (b_{\mathrm{B}} + b_{\mathrm{F}})\frac{f}{3} + \frac{f^2}{5}\right]C_0(d) + \frac{1}{5}\left[(b_{\mathrm{B}} + b_{\mathrm{F}})\frac{2f}{3} + \frac{4f^2}{7}\right]C_2(d)\Bigg\}\,. \tag{17}$$

The large-angle dipole (17) has a different physical origin than the wide-angle dipole (12). As explained above, the wide-angle dipole is due to the fact that the two-point function is intrinsically anti-symmetric in the full sky due to the difference between the line-of-sight to the bright and to the faint galaxies. The large-angle dipole on the other hand is due to the fact that the angle we are using to measure the dipole breaks explicitly the symmetry of the situation. From this we understand already that the large-angle dipole exists also in the case where we have only *one* population of galaxies. In section 3.5 we will show how this term can be measured in that case.

In figure 3 we compare the different dipole contributions at $z = 0.30$ and $z = 0.58$ using the angle σ and β. These contributions depend on the bias of the bright and faint populations. We use the values measured in section 3 to evaluate them. The dipole due to evolution depends furthemore on the evolution of the bias for which we need a model. However, as shown in figure 11 of Bonvin et al. (2014) this contribution is much smaller than the relativistic, wide-angle and large-angle dipoles. Therefore we can safely neglect it. Figure 3 shows that the large-angle contribution (measured with β) is significantly larger than the other contributions.

3 MEASUREMENTS OF THE DIPOLE

We now apply our method to the BOSS survey. We measure the monopole and the dipole in the LOWz and CMASS samples, data release DR10 (Anderson et al. 2014). In each sample, we split the population of galaxies into a bright and a faint population. In order to obtain a homogeneous fraction of bright and faint galaxies over the samples, we divide them

[5] Note that this large-angle contribution also affects the monopole and quadrupole and it is sometimes included into the wide-angle contribution (see e.g. Reimberg et al. (2015)).

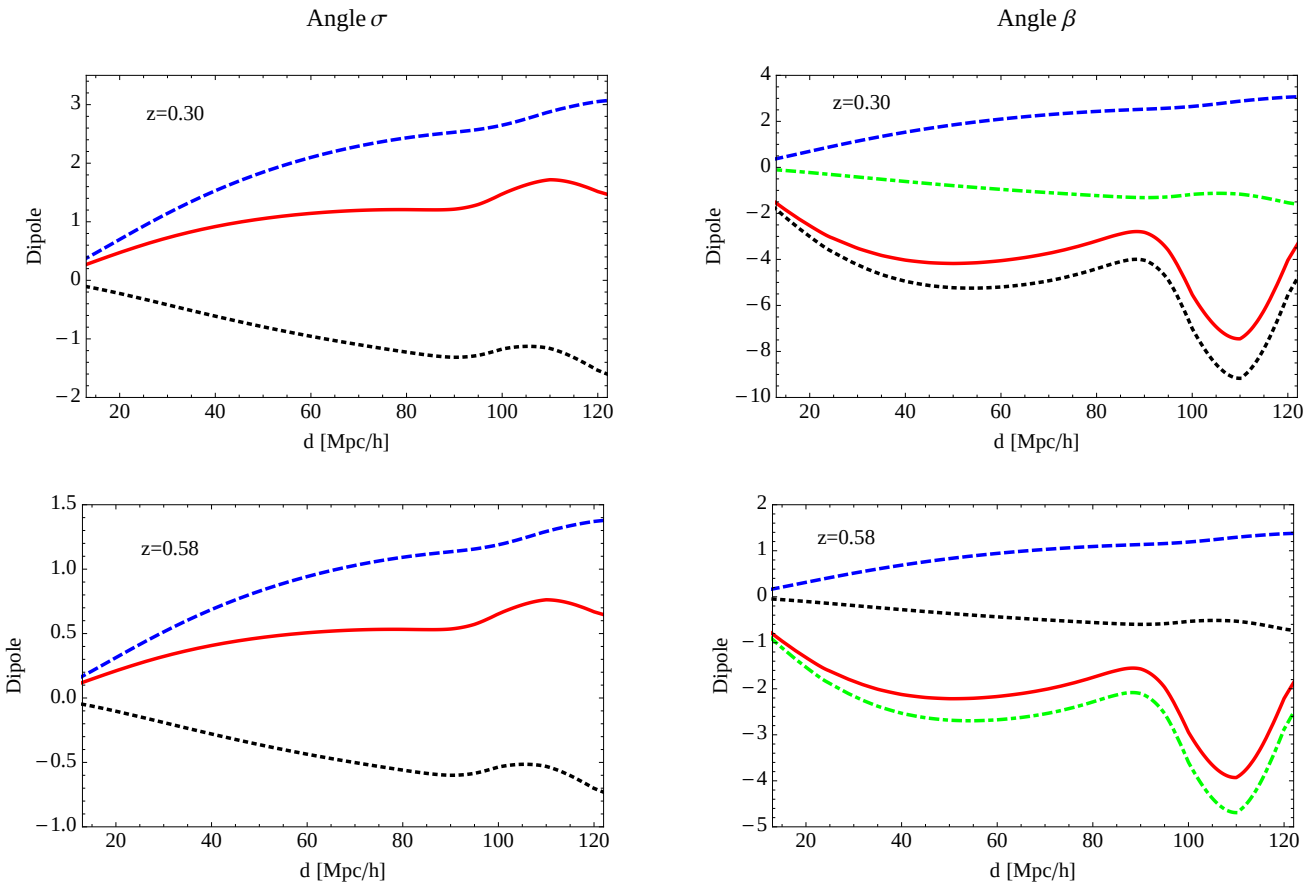

Figure 3. Predictions for the observed dipole at $z = 0.30$ and $z = 0.58$, multiplied by d^2, and plotted as a function of separation. In the left panels we show the dipole measured with $\mu_1 \equiv \cos\sigma$ and in the right panels with $\mu_{12} \equiv \cos\beta$. The blue dashed line is the relativistic dipole, the black dotted line is the wide-angle dipole, the green dot-dashed line is the large-angle dipole and the red solid line is the total. The dipole due to evolution is much smaller than the other contributions and we have therefore neglected it. Note that the scale on the y-axis is different for each plot.

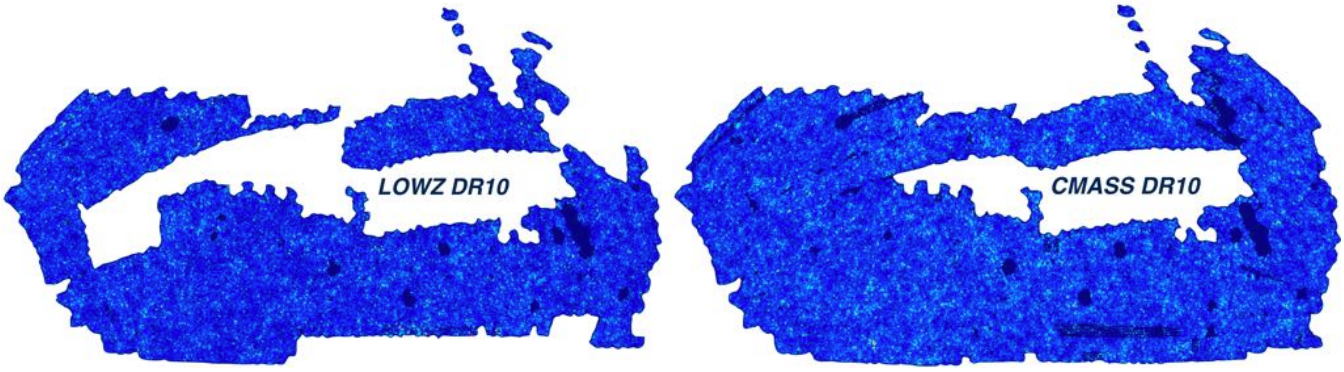

Figure 4. Distribution of galaxies in the LOWz and the CMASS samples. Weights are included.

into sub-samples of width $\Delta z \simeq 0.01$ and we adjust the luminosity cut in each sub-sample to have roughly equal numbers of bright and faint galaxies. With this procedure, we obtain for both samples $\bar{n}_{\rm B} = 0.47$ and $\bar{n}_{\rm F} = 0.53$. In LOWz we use 148'833 galaxies and in CMASS 380'899 galaxies. In both samples we use cubic pixels with size $\ell_p = 4\,{\rm Mpc}/h$ for separations $16 \leq d \leq 120\,{\rm Mpc}/h$. The effective redshift of the LOWz sample is $\bar{z} = 0.303$ and of the CMASS sample $\bar{z} = 0.575$.

We weight galaxies according to the prescriptions given in Anderson et al. (2014) and we use the public LSS random catalogs to build the masks. The distribution of galaxies is shown in figure 4 for both the LOWz and the CMASS samples. We pixelize the samples in 3D cubical pixels and estimate the correlation function, as explain around eq. (3).

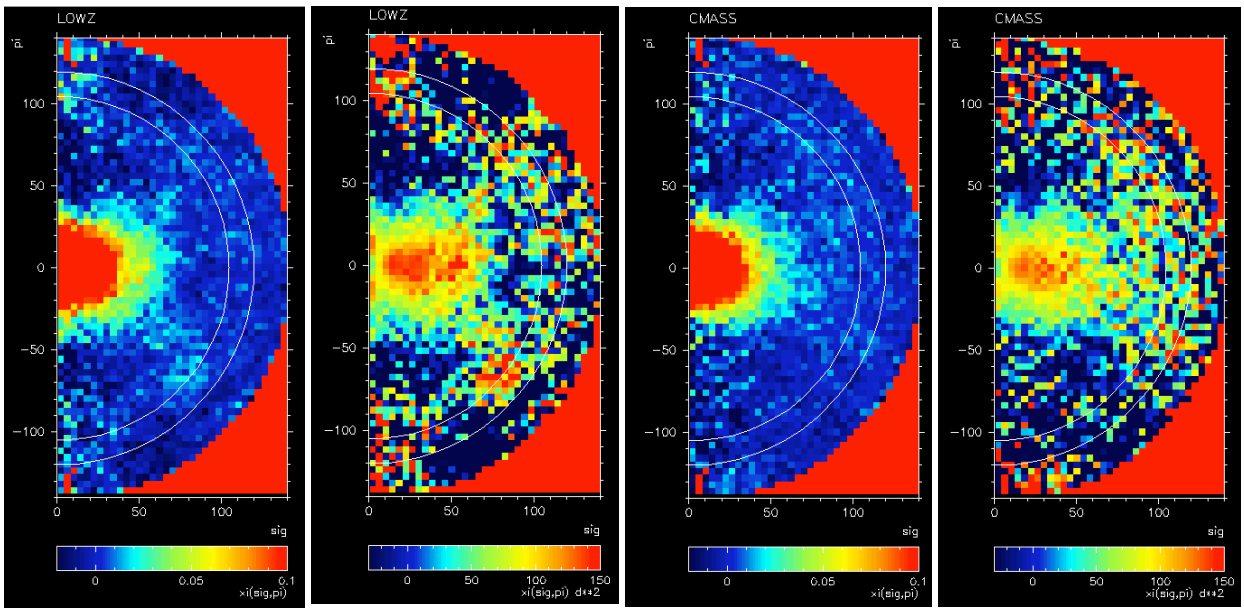

Figure 5. 2D cross-correlation function using the angle σ_{ij}, plotted as a function of parallel (y-axis) and perpendicular (x-axis) separation with respect to the line-of-sight. The two left panels show the cross-correlation function in the LOWz sample and the two right panels in the CMASS sample. In the first and third panels we directly plot the cross-correlation function, whereas in second and fourth panels we plot the cross-correlation function multiplied by d^2.

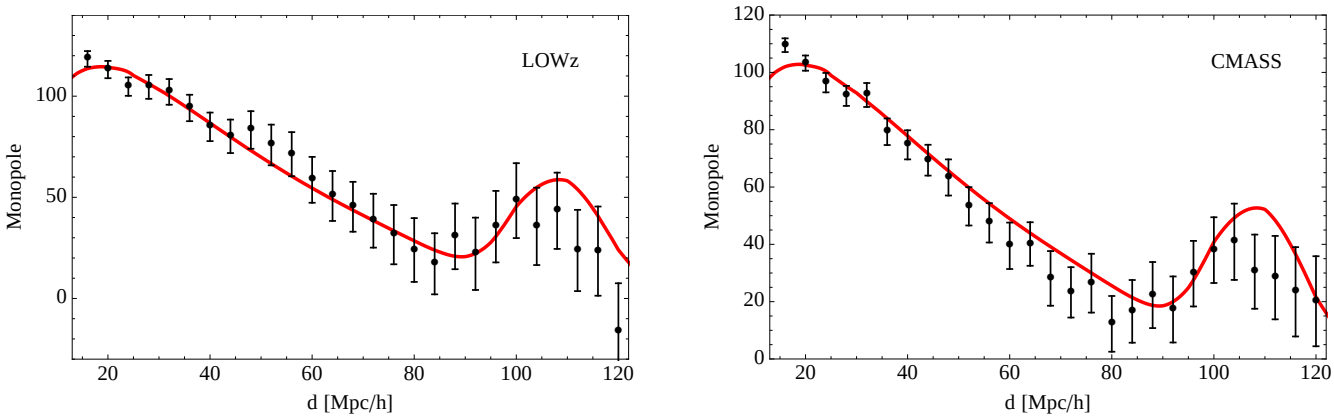

Figure 6. Measurements of the monopole (multiplied by d^2) from the cross-correlation of bright and faint galaxies in the LOWz and CMASS samples, plotted as a function of separation. The red solid line is the prediction using linear perturbation theory.

We bin the correlation in both separation and line-of-sight angle, using the angle σ_{ij} and β_{ij}. We use 329 Jack-knife (JK) regions in LOWz and 335 JK regions in CMASS to evaluate the error-bars in the data. The resulting 2D cross-correlations are shown in figure 5 for the angle σ_{ij}, as a function of parallel and perpendicular separation with respect to the line-of-sight (see Gaztanaga et al. 2009). Note that contrary to the plots shown in Gaztanaga et al. (2009), the plots in figure 5 are not symmetric in the parallel separation because we always use the bright galaxy as the centre to measure the angle and distinguish between positive and negative line-of-sight separation. This allows us to measure the multipoles as projection over Legendre polynomials. Also note in the figure some significant large scale "noise" on scales 50-100 Mpc/h. This is partially due to the fact that we are measuring cross-correlations of bright and faint galaxies. These galaxies do not have the same redshift distribution or trace matter in exactly the same way, which creates some additional noise and modulation compared to the auto-correlations, particularly at large separations (this could be called relative bias "stochasticity"). Also, note that especially for the LOWz sample, the pairs at large negative radial separation are sampling smaller volumes than the ones at positive values. This results in an enhancement of sam-

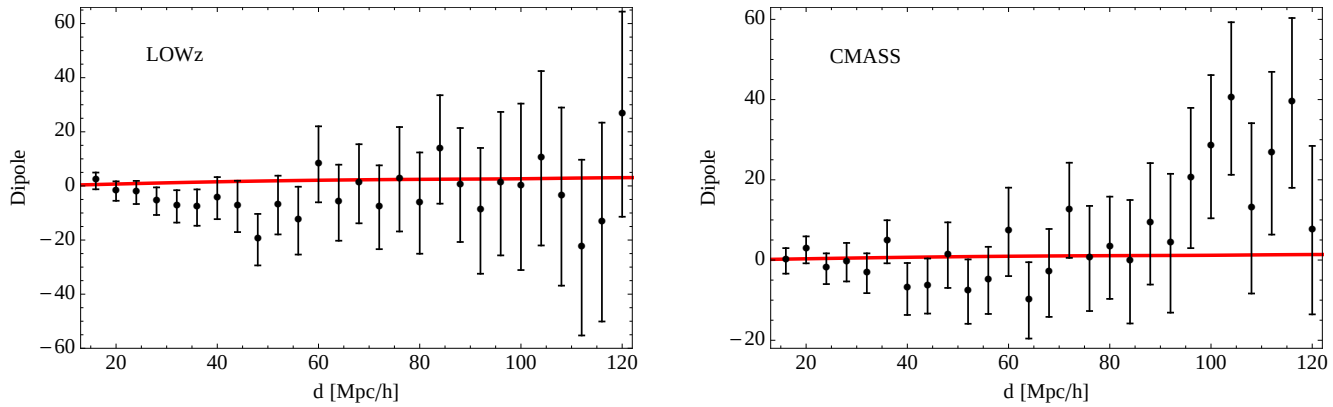

Figure 7. Measurements of the dipole using the median angle $\mu_{12} = \cos\sigma$, multiplied by d^2, from the cross-correlation of bright and faint galaxies in the LOWz and CMASS samples, plotted as a function of separation. The red solid line is the prediction using linear perturbation theory and the biases $b_{\rm B}$ and $b_{\rm F}$ are fitted from the total and cross monopoles, eqs. (18) and (19).

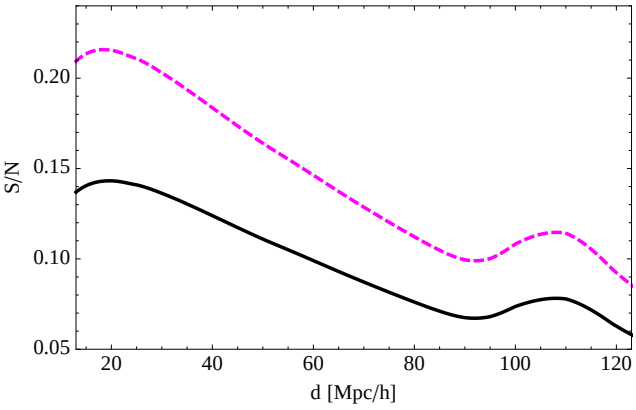

Figure 8. Signal-to-noise for the dipole using the median angle $\mu_{12} = \cos\sigma$, in the LOWz sample (magenta dashed line) and in the CMASS sample (black solid line), plotted as a function of separation.

pling variance around BAO position, as shown by the broad structure at separations (-70 radial , +70 perpendicular) in the LOWz panels [6].

We measure the monopole using all pairs of galaxies $\zeta_0^{\rm T}(d)$ (i.e. without distinguishing bright and faint galaxies) and then using only the cross-correlation between bright and faint galaxies $\zeta_0(d)$. We compare these measurements with linear predictions using the fiducial cosmological parameters of Anderson et al. (2014) ($\Omega_m = 0.274$, $h = 0.7$, $\Omega_b h^2 = 0.0224$, $n_s = 0.95$ and $\sigma_8 = 0.8$) to find the respective bias of the two populations

$$\zeta_0^{\rm T}(d) = \left[b_{\rm T}^2 + 2b_{\rm T}\frac{f}{3} + \frac{f^2}{5}\right] C_0(d)\,, \quad (18)$$

$$\zeta_0(d) = \left[b_{\rm B}b_{\rm F} + (b_{\rm B}+b_{\rm F})\frac{f}{3} + \frac{f^2}{5}\right] C_0(d)\,, \quad (19)$$

where the bias of the whole sample $b_{\rm T}$ is related to the bias of the bright and faint populations by

$$b_{\rm T} = \bar{n}_{\rm B} b_{\rm B} + \bar{n}_{\rm F} b_{\rm F}\,. \quad (20)$$

In LOWz we find $b_{\rm B} = 2.30 \pm 0.21$ and $b_{\rm F} = 1.31 \pm 0.21$; and in CMASS we find $b_{\rm B} = 2.36 \pm 0.18$ and $b_{\rm F} = 1.46 \pm 0.18$. We then use these values to predict the amplitude of the dipole. Note that this method is more robust than fitting the bias using separately the monopole from the bright $\zeta_0^{\rm B}(d)$ and the monopole from the faint $\zeta_0^{\rm F}(d)$. The reason is that the weights defined in Anderson et al. (2014) are constructed for the whole population. Applying these weights separately to the bright and faint populations generates inhomogeneous samples. This significantly affects the measurement of the bright and faint monopoles. The measurement of the cross-correlation between the bright and the faint populations is however relatively insensitive to this problem and it provides therefore a more robust way of extracting the biases.

In figure 6 we show the measurements of the monopole for the cross-correlations between the bright and the faint populations in the LOWz and CMASS samples. The red line represents the theoretical prediction.

3.1 Measurement of the dipole using the median angle $\mu_{12} \equiv \cos\sigma$

We start by measuring the dipole with the median angle $\mu_{12} = \cos\sigma$. In figure 7 we show the dipole in the LOWz and CMASS samples. In both cases, the dipole is compatible with zero within the error bars.

In Bonvin et al. (2015), we have calculated the errors on the dipole due to Poisson sampling and cosmic variance. We found that the diagonal part of the error can be written as [7]

$$\text{error} = \left(\frac{3}{4\pi N_{\rm tot}(\bar{n}_{\rm B}\bar{n}_{\rm F})^2}\right)^{1/2} \times \left[\frac{\bar{n}_{\rm B}\bar{n}_{\rm F}}{\bar{N}d^2\ell_p} + \frac{3}{2}\Big(D_0\sigma_0(d) + D_2\sigma_2(d) + D_4\sigma_4(d)\Big)\right]^{1/2}, \quad (21)$$

[6] This geometrical effect could help explaining the results in Cabre & Gaztanaga (2011), which shows how the BAO position could be well measured even at instances where sampling variance does not allow to favor a model with BAO peak from one without it.

[7] Note that to be consistent with the normalisation a_N used here, we must divide eqs. (43) and (44) of Bonvin et al. (2015) by $\left(N_{\rm tot}\ell_p d^2 \bar{N}\bar{n}_{\rm B}\bar{n}_{\rm F}\right)^2$.

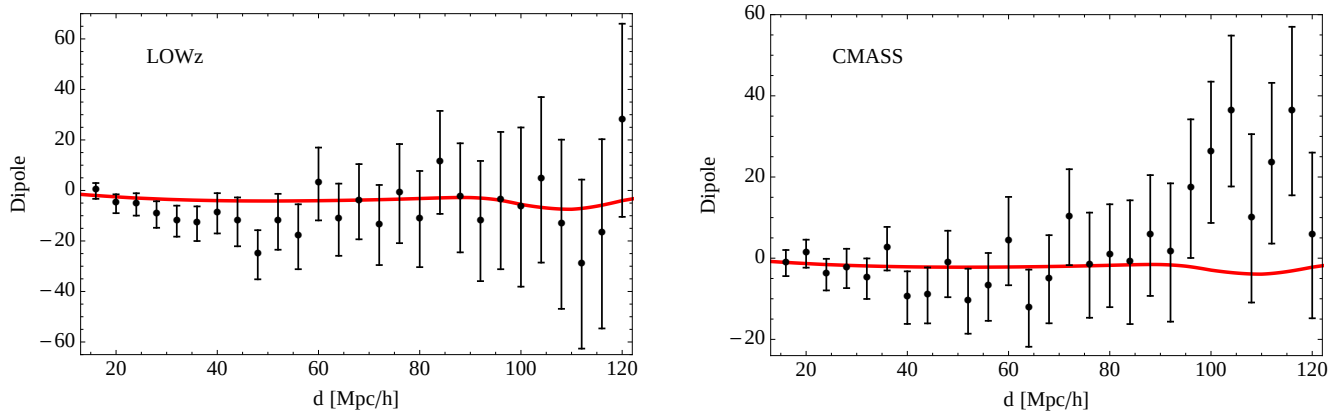

Figure 9. Measurements of the dipole using the angle from the bright galaxy $\mu_1 = \cos\beta$, multiplied by d^2, from the cross-correlation of bright and faint galaxies in the LOWz and CMASS samples, plotted as a function of separation. The red solid line is the prediction using linear perturbation theory and the biases $b_{\rm B}$ and $b_{\rm F}$ are fitted from the total and cross monopoles, eqs. (18) and (19).

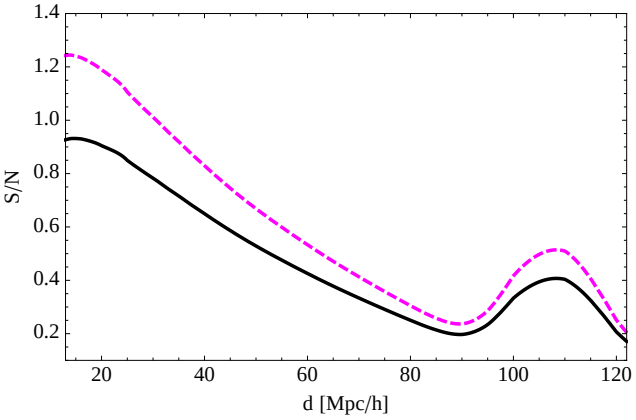

Figure 10. Signal-to-noise for the dipole using the angle from the bright galaxy $\mu_1 = \cos\beta$, in the LOWz sample (magenta dashed line) and in the CMASS sample (black solid line), plotted as a function of separation.

where

$$\sigma_\ell(d) = -\frac{1}{2\pi^2}\int_{-1}^{1} d\rho\,\rho \int_{-1}^{1} d\nu\,\nu \int_0^{2\pi} d\varphi \qquad (22)$$
$$\times \int dk k^2 P(k,\bar z) j_\ell(ks) P_\ell\left(\frac{d(\rho+\nu)}{s}\right), \quad \ell = 0,2,4$$

with P_ℓ the Legendre polynomial of degree ℓ and

$$s = d\sqrt{2\left(1+\rho\nu+\sqrt{(1-\rho^2)(1-\nu^2)}\sin\varphi\right)}. \qquad (23)$$

For two populations of galaxies we have

$$\begin{aligned} D_0 &= \bar n_{\rm B}^2\bar n_{\rm F}\left(b_{\rm B}^2+\frac{2b_{\rm B}f}{3}+\frac{f^2}{5}\right)+\bar n_{\rm F}^2\bar n_{\rm B}\left(b_{\rm F}^2+\frac{2b_{\rm F}f}{3}+\frac{f^2}{5}\right),\\ D_2 &= -\bar n_{\rm B}^2\bar n_{\rm F}\left(\frac{4b_{\rm B}f}{3}+\frac{4f^2}{7}\right)-\bar n_{\rm F}^2\bar n_{\rm B}\left(\frac{4b_{\rm F}f}{3}+\frac{4f^2}{7}\right),\\ D_4 &= \left(\bar n_{\rm B}^2\bar n_{\rm F}+\bar n_{\rm F}^2\bar n_{\rm B}\right)\frac{8f^2}{35}. \end{aligned} \qquad (24)$$

Using these expressions we can calculate the signal-to-noise for the dipole in the LOWz and in the CMASS samples. Since the number densities and the fraction of bright and faint galaxies evolve with redshift, we split each of the samples into 3 redshift bins. We calculate the signal-to-noise in each bin and then add them in quadrature to obtain the total signal-to-noise (note that to a very good approximation the different redshift bins are uncorrelated). We plot the results in figure 8. The signal-to-noise is very small showing that no detection of the dipole is possible using the median angle. Note that the signal-to-noise calculated here is the signal-to-noise at fixed separation d. The cumulative signal-to-noise combining all separations can be calculated using eq. (55) of Bonvin et al. (2015).

3.2 Measurement of the dipole using the angle from the bright galaxy $\mu_1 \equiv \cos\beta$

We then measure the dipole using the angle from the bright galaxy $\mu_1 \equiv \cos\beta$. As shown in figure 3, with this choice of kernel the dipole is much larger that with the median angle σ, due to the existence of the large-angle dipole. In figure 9 we show the dipole in the LOWz and CMASS samples. Even though the signal is much larger in this case, the errors are still too large to allow for a detection of the large-angle dipole. In figure 10 we show the predicted signal-to-noise in this case, which is of order 1 at small separation.

3.3 Measurement of the large-angle dipole using the angle difference $\mu_1 - \mu_{12} = \cos\beta - \cos\sigma$

From eqs. (7), (8), (12) and (16), we see that we can construct a new kernel to isolate the large-angle effect. Indeed using

$$w_{\mathbf{x}_i\mathbf{x}_j L_i L_j} = a_N\left(\cos\beta_{ijL_iL_j} - \cos\sigma_{ijL_iL_j}\right)\delta_K(d_{ij}-d), \qquad (25)$$

we obtain

$$\begin{aligned} \langle\hat\xi\rangle &= -a_N d\bar n_{\rm B} d\bar n_{\rm F}\sum_{ij}\langle\Delta_{\rm B}(\mathbf{x}_j)\Delta_{\rm F}(\mathbf{x}_i)\rangle\frac{d_{ij}}{r_i}(1-\cos^2\beta_{ij})\delta_K(d_{ij}-d)\\ &= \langle\hat\xi^{\rm large}\rangle = \frac{d}{r}\left[\zeta_0(d)-\frac{1}{5}\zeta_2(d)\right], \end{aligned} \qquad (26)$$

where ζ_0 is the monopole defined in eq. (19) and ζ_2 is the quadrupole given by

$$\zeta_2(d) = -\left[(b_{\rm B}+b_{\rm F})\frac{2f}{3}+\frac{4f^2}{7}\right]C_2(d). \qquad (27)$$

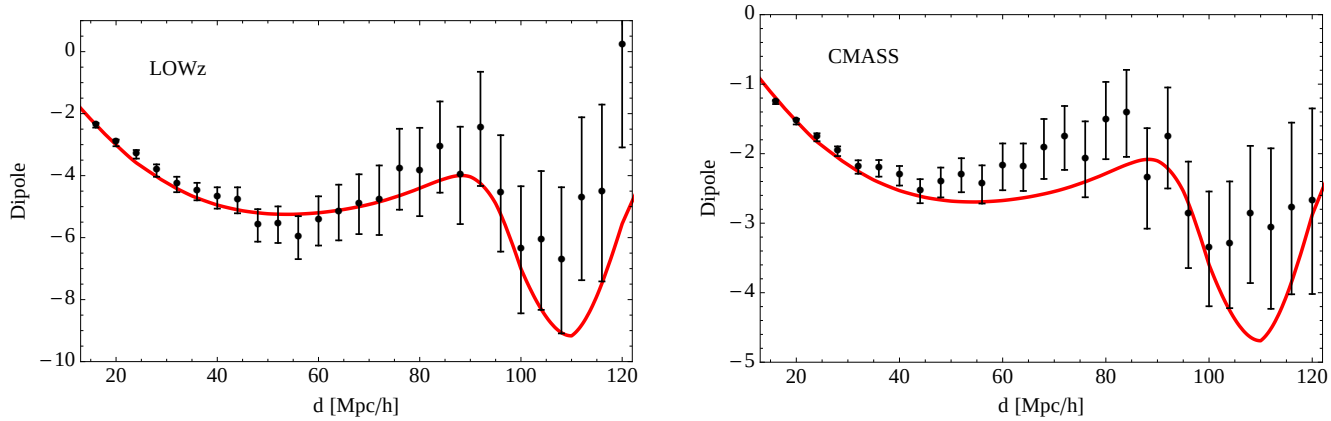

Figure 11. Measurements of the dipole using $\mu_1 - \mu_{12} = \cos\beta - \cos\sigma$ (kernel (25)), multiplied by d^2, from the cross-correlation of bright and faint galaxies in the LOWz and CMASS samples, plotted as a function of separation. The red solid line is the prediction using linear perturbation theory and the biases $b_{\rm B}$ and $b_{\rm F}$ are fitted from the total and cross monopoles, eqs. (18) and (19).

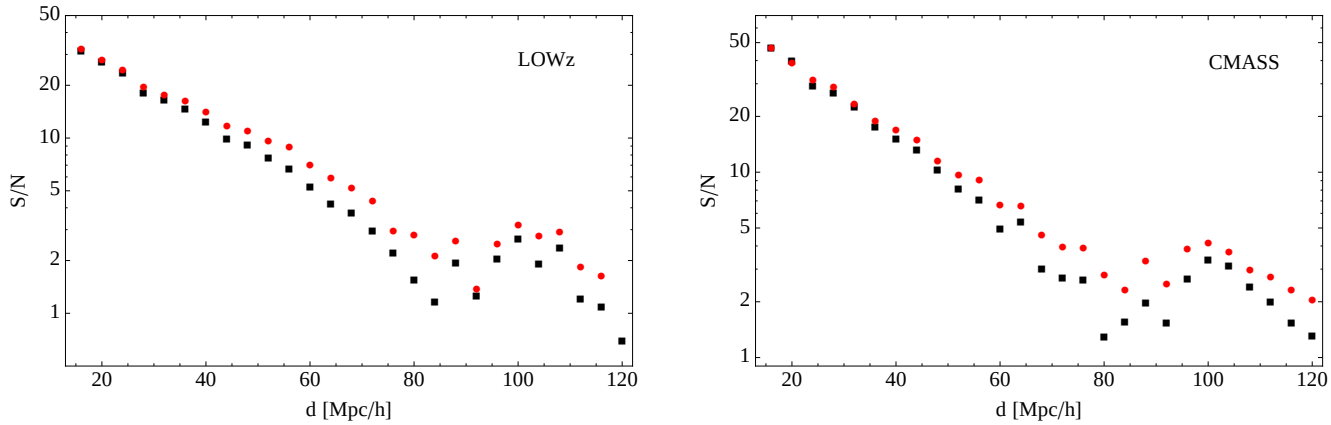

Figure 12. Signal-to-noise of the dipole (red dots) measured using $\mu_1 - \mu_{12} = \cos\beta - \cos\sigma$ from the cross-correlation of bright and faint galaxies in the LOWz and CMASS samples, plotted as a function of separation. The black squares represent the signal-to-noise of the monopole obtained from the same samples.

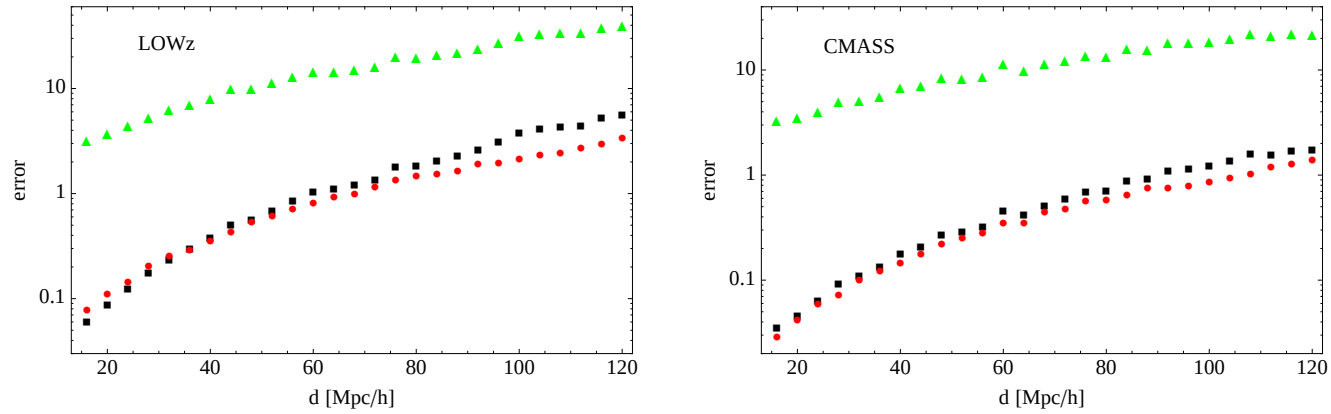

Figure 13. Error on the dipole measured from the cross-correlation of bright and faint galaxies in the LOWz and CMASS samples, plotted as a function of separation. The red dots show the error obtained with the angle $\mu_1 - \mu_{12} = \cos\beta - \cos\sigma$ and the green triangles show the error obtained with the angle $\mu_1 = \cos\beta$. The black squares are obtained by multiplying the green triangles by d/r.

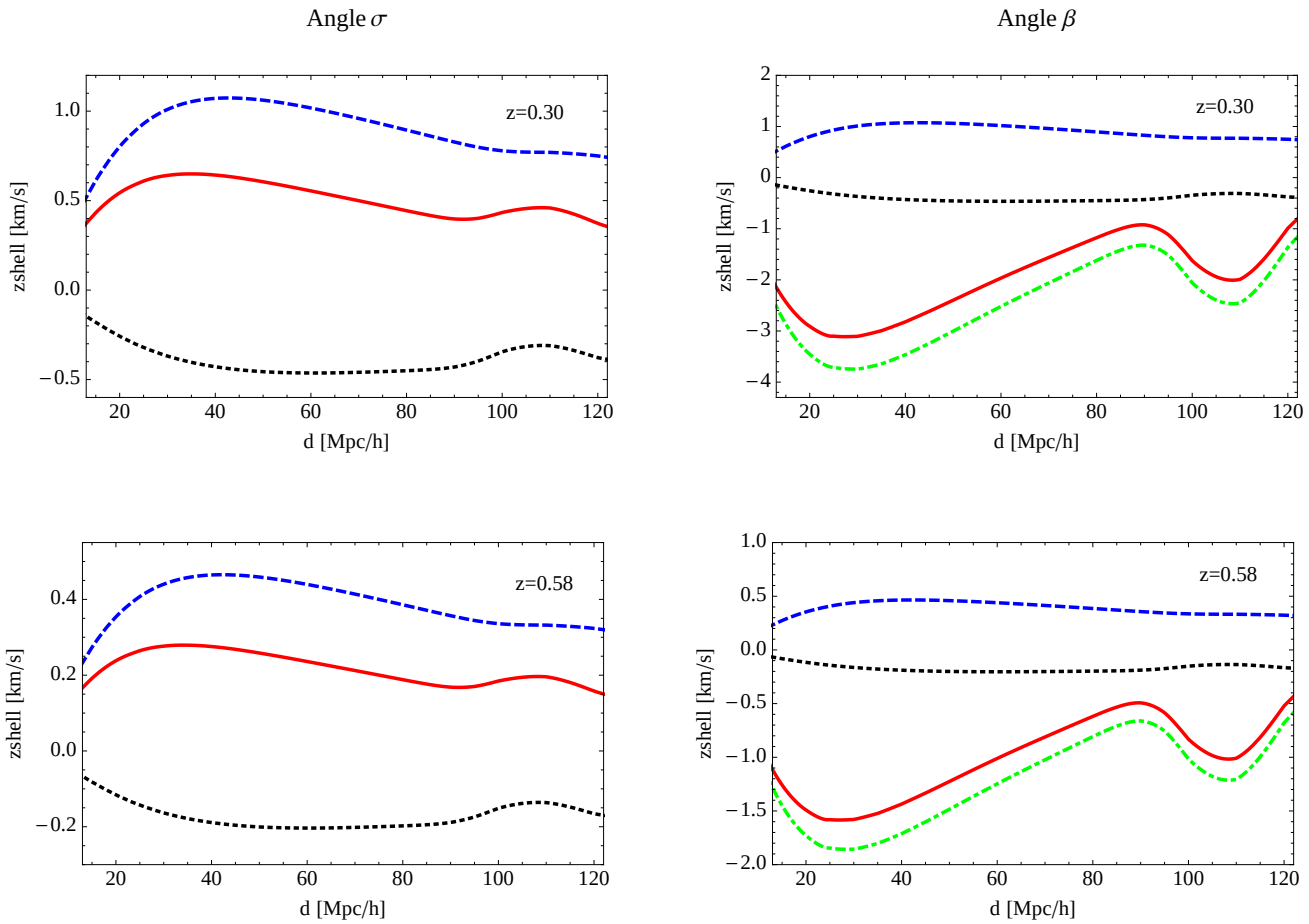

Figure 14. Predictions for the estimator $z_{\rm shell}$ at $z = 0.30$ and $z = 0.58$, plotted as a function of separation. In the left panels we show $z_{\rm shell}$ calculated with the angle $\mu_{12} = \cos\sigma$ and in the right panels with $\mu_1 = \cos\beta$. The blue dashed line is the relativistic contribution, the black dotted line is the wide-angle contribution, the green dot-dashed line is the large-angle contribution and the red solid line is the total.

The relativistic dipole, the dipole due to evolution and the wide-angle dipole are therefore totally absent with this choice of kernel: only the large-angle effect contributes. In figure 11 we show the dipole measured with this new kernel in the LOWz and CMASS samples. We have a very clear detection of the large-angle dipole, which agrees well with the predictions in both samples.

The signal-to-noise for the dipole is very large. As shown in figure 12, it is comparable to the signal-to-noise of the monopole. This is due to the fact that the combination of angles $\mu_1 - \mu_{12}$ removes the dominant part of the variance. Using kernel (25) the variance of the dipole can indeed be written as

$$\mathrm{var}(\hat{\xi}^{\rm large}) = 2a_N^2 \sum_{ijL_iL_j} \sum_{abL_aL_b} \delta_K(d_{ij}-d)\delta_K(d_{ab}-d)$$
$$\times \left(\cos\beta_{ijL_iL_j} - \cos\sigma_{ijL_iL_j}\right)\left(\cos\beta_{abL_aL_b} - \cos\sigma_{abL_aL_b}\right)$$
$$\times \langle \delta n_{L_i}(\mathbf{x}_i)\delta n_{L_a}(\mathbf{x}_a)\rangle\langle \delta n_{L_j}(\mathbf{x}_j)\delta n_{L_b}(\mathbf{x}_b)\rangle\,. \qquad (28)$$

In the distant-observer approximation $\cos\beta_{ijL_iL_j} = \cos\sigma_{ijL_iL_j}$ and $\cos\beta_{abL_aL_b} = \cos\sigma_{abL_aL_b}$ so that the variance exactly vanishes. This similarity in the variance is clearly visible if we compare figures 7 and 9. The amplitude of the error bars as well their variation with separation look exactly the same. As a consequence with kernel (25) the only contribution to the variance is from large-angle effects, which are suppressed by a factor d/r. This suppression is illustrated in figure 13.

To summarise, our analysis shows that the large-angle dipole is significantly larger than the relativistic dipole, the evolution dipole and the wide-angle dipole. This large-angle dipole exists only if we use the angle $\mu_1 = \cos\beta$ in our estimator. To measure this effect in BOSS it is however not sufficient to simply weight the two-point function by $\cos\beta$, since in this case the error on the dipole is affected by flat-sky contributions. To remove this large error we need to choose our estimator such that the dipole exactly vanishes in the distant-observer approximation. Kernel (25) satisfies this constraint and allows us to measure the large-angle dipole with a signal-to-noise of more than 50. Note that this value refers to the signal-to-noise per bin of separation. The cumulative signal-to-noise over the whole range of separation is even larger.

3.4 Comparison with the estimator $z_{\rm shell}$

In Croft (2013), Croft constructed an estimator $z_{\rm shell}$ to measure the redshift difference generated by gravitational redshift in large-scale structure. Writing the parallel separation

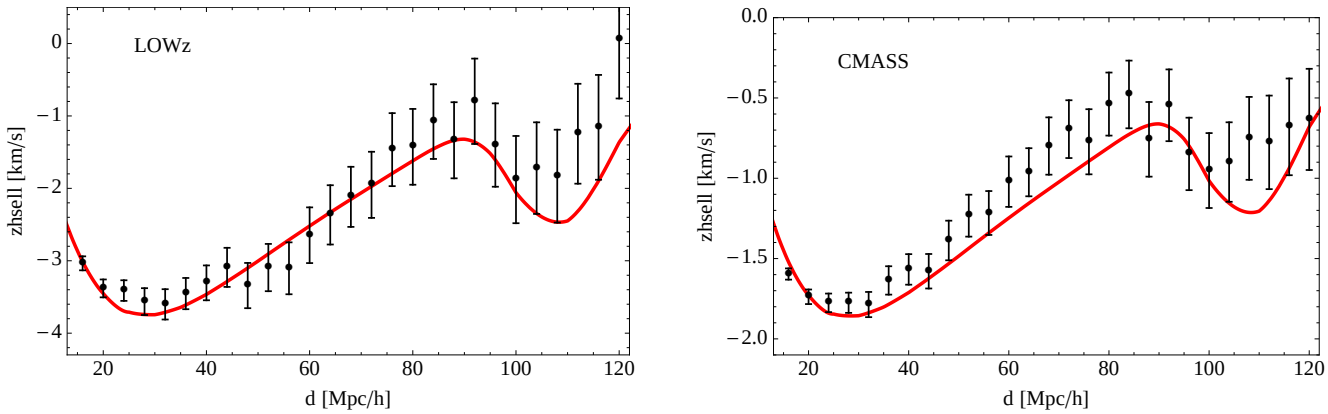

Figure 15. Measurements of $z_{\rm shell}$ using $\mu_1 - \mu_{12} = \cos\beta - \cos\sigma$, from the cross-correlation of bright and faint galaxies in the LOWz and CMASS samples, plotted as a function of separation. The red solid line is the prediction using linear perturbation theory and the biases $b_{\rm B}$ and $b_{\rm F}$ are fitted from the total and cross monopoles, eqs. (18) and (19).

between galaxies as $d\cos\gamma$ and integrating over the orientation of the pair $\mu = \cos\gamma$, eq. (9) in Croft (2013) can be rewritten as

$$z_{\rm shell} = \frac{\int_{-1}^{1} d\mu \int_{d}^{d+\Delta d} ds\, s^3 \mu H \zeta(s,\mu)}{\int_{-1}^{1} d\mu \int_{d}^{d+\Delta d} ds\, s^2 (1+\zeta(s,\mu))} = \frac{1}{3}\frac{\int_{d}^{d+\Delta d} ds\, s^3 H \zeta_1(s)}{\int_{d}^{d+\Delta d} ds\, s^2 (1+\zeta_0(s))}\,, \tag{29}$$

where $H = \mathcal{H}/a$ is the Hubble parameter, ζ is the two-point correlation function of galaxies and ζ_0 and $\zeta_1 = \langle\hat{\xi}\rangle$ denote respectively the monopole and dipole contributions. For Δd sufficiently small, we can assume that the integrand is constant and we find

$$z_{\rm shell} \simeq \frac{1}{3}\frac{dH(\bar{z})\langle\hat{\xi}\rangle(d)}{1+\zeta_0(d)}\,. \tag{30}$$

The estimator $z_{\rm shell}$ can therefore easily be calculated using our expression for the dipole. In figure 14 we show the predictions for the different contributions to $z_{\rm shell}$ at $z = 0.30$ and $z = 0.58$, using $\mu_{12} = \cos\sigma$ and $\mu_1 = \cos\beta$. We see that the relativistic distortions generate a redshift difference $z_{\rm shell}$ of the order of 1 km/s at low redshift and 0.4 km/s at high redshift. Using the angle β on the other hand, the large-angle effect produces a redshift difference of the order of -4 km/s at low redshift and -2 km/s at high redshift. In figure 15 we show measurements of $z_{\rm shell}$ in the LOWz and CMASS samples using $\mu_1 - \mu_{12}$ to isolate the large-angle effect. As for the dipole, a significant detection of the large-angle effect in $z_{\rm shell}$ is possible due to the cancellation of the flat-sky part of the error.

This measurement of the large-angle effect in $z_{\rm shell}$ should be distinguished from the measurements of Wojtak et al. (2011); Sadeh et al. (2015) using clusters of galaxies. Wojtak et al. (2011) measured the redshift difference between the brightest galaxies at the centre of clusters and the other members of the clusters in the SDSS data release DR7. They found a mean difference of -7.7 ± 3 km/s. Sadeh et al. (2015) performed a similar analysis in the SDSS data release DR10, and found a mean redshift difference of $-11 + 7 - 5$ km/s. These measurements have been compared with the mean redshift difference predicted by gravitational redshift and found to be consistent (note however the discussion in Zhao et al. (2013); Kaiser (2013), which emphasises the importance of non-linear velocity contributions). From figure 14 and 15, we see that with the estimator $z_{\rm shell}$ we are able to measure the large-angle effect but not the relativistic contribution (which includes the gravitational redshift effect). The relativistic contribution to $z_{\rm shell}$ is indeed of the order of 1 km/s in the LOWz sample, i.e. ~ 10 times smaller than the redshift difference measured in clusters. It has also the opposite sign with respect to the redshift difference in clusters.

As explained in Bonvin et al. (2014) (see appendix E), this difference between the measurements from clusters and the ones from large-scale structure comes from the fact that clusters do have a physical boundary. This boundary is used in the measurement of the redshift difference, which is averaged from the minimal redshift of the cluster $z_{\rm min}$ to the maximal redshift of the cluster $z_{\rm max}$. The dominant effect in the measurement comes then from the asymmetric shift in the cluster's boundaries due to gravitational redshift: $z_{\rm max} - z_{\rm B} < z_{\rm B} - z_{\rm min}$. As shown in Bonvin et al. (2014), this effect is in reality a three-point correlation function $\langle\Delta_{\rm B}\Delta_{\rm F}\partial_r\Psi\rangle$ and it is negative. On the other hand, in large-scale structure we do not have a natural boundary within which we can integrate the estimator $z_{\rm shell}$. Therefore the average is performed over a symmetric boundary in redshift-space: in (29) the two-point function is averaged within a symmetric shell of width Δd situated at distance d from the central galaxy. The effect which is measured through $z_{\rm shell}$ (and similarly through the dipole) is therefore the effect of gravitational redshift on the two-point correlation function directly and not on the boundary of the shell. From figure 14 we see that this effect is much smaller than the boundary effect and of opposite sign. This explains why it is more difficult to measure gravitational redshift in large-scale structure than in clusters.

3.5 Large-angle dipole in a single population of galaxies

The relativistic, evolution and wide-angle dipoles all vanish in the case where we have only one population of galaxies.

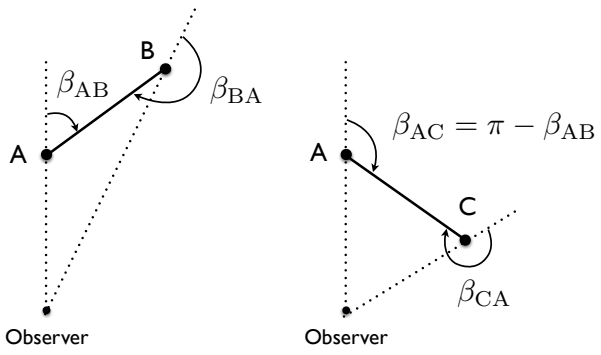

Figure 16. The contribution AB cancels with the contribution AC, since $\cos\beta_{\rm AC} = -\cos\beta_{\rm AB}$. However at large separation, the contribution CA does not cancel with the contribution BA, since $\cos\beta_{\rm CA} \neq -\cos\beta_{\rm BA}$.

This is clearly visible from eqs. (7), (8) and (12) which show that these effects are sensitive to the bias difference between the two populations of galaxies. The large-angle dipole on the other hand does not depend on the bias difference between the populations, see eq. (17). As such this effect should also exist in a single population of galaxies.

With one population of galaxies, we can construct the following estimator

$$\hat{\xi} = a_N \sum_{ij} \delta n(\mathbf{x}_i)\delta n(\mathbf{x}_j) \cos\gamma_{ij} \delta_K(d_{ij} - d)\,. \quad (31)$$

Since there is no distinction between the two galaxies in the pair we always define the angle γ_{ij} with respect to the first pixel i. Each pair will automatically be counted twice: for example a pair A-B will contribute as

$$\xi_{\rm AB} = a_N d\bar{n}^2 \Delta_{\rm A}\Delta_{\rm B} \left(\cos\gamma_{\rm AB} + \cos\gamma_{\rm BA}\right) \delta_K(d_{\rm AB} - d)\,, \quad (32)$$

where in $\Delta_{\rm A}$ and $\Delta_{\rm B}$ we include only the standard density and redshift-space distortions since we know that the relativistic effects vanish for one population (at lowest order in d/r). From figure 1 we see that if we choose $\gamma = \sigma$ then $\sigma_{\rm BA} = \sigma_{\rm AB} + \pi$ so that

$$\cos\sigma_{\rm AB} + \cos\sigma_{\rm BA} = 0\,, \quad (33)$$

and the contribution from *each* pair exactly vanishes. If on the other hand we choose $\gamma = \beta$, then $\cos\beta_{\rm BA} \neq -\cos\beta_{\rm AB}$ and the contribution does not vanish. From eq. (14) we obtain

$$\xi_{\rm AB} = -a_N d\bar{n}^2 \Delta_{\rm A}\Delta_{\rm B} \frac{d_{\rm AB}}{r} \left(1 - \cos^2\beta_{\rm AB}\right) \delta_K(d_{\rm AB} - d)\,. \quad (34)$$

Summing over all pairs (i.e. integrating over all orientations), we obtain then

$$\langle\hat{\xi}\rangle = \langle\hat{\xi}^{\rm large}\rangle = \frac{d}{r}\left[\zeta_0(d) - \frac{1}{5}\zeta_2(d)\right]\,. \quad (35)$$

This result may seem counter-intuitive: one could indeed argue that since we multiply by a cosine, for each pair A-B there exist another pair A-C with an opposite cosine which should cancel with A-B. This is however not correct at large separation. From figure 16 we see that if we choose C such that $\cos\beta_{\rm AC} = -\cos\beta_{\rm AB}$ we remove only the first contribution to the pair. We have indeed

$$\xi_{\rm AB} + \xi_{\rm AC} = a_N d\bar{n}^2 \Big[\Delta_{\rm A}\Delta_{\rm B}\big(\cos\beta_{\rm AB} + \cos\beta_{\rm BA}\big)\delta_K(d_{\rm AB} - d) + \Delta_{\rm A}\Delta_{\rm C}\big(\cos\beta_{\rm AC} + \cos\beta_{\rm CA}\big)\delta_K(d_{\rm AC} - d)\Big]\,. \quad (36)$$

Since at fixed separation d, $\Delta_{\rm A}\Delta_{\rm B} = \Delta_{\rm A}\Delta_{\rm C}$, the first term in the first line of eq. (36) cancels with the first term in the second line. However the second terms do not cancel because

$$\cos\beta_{\rm BA} + \cos\beta_{\rm CA} = -2\frac{d}{r}\left(1 - \cos^2\beta_{\rm AB}\right) \neq 0\,. \quad (37)$$

Therefore in the full-sky there is no pair which exactly cancels the contribution from the pair A-B. Note that the existence of a large-angle dipole in one population of galaxies has already been demonstrated in Reimberg et al. (2015).

We measure the large-angle dipole with one population in the LOWz and CMASS samples. As for two populations, we use the combination of angle $\cos\beta - \cos\sigma$ to remove the dominant part of the cosmic variance (see section 3.3). The results are plotted in figure 17. We see that the dipole agrees very well with the predictions both in the LOWz and in the CMASS samples. Since contrary to the case of two populations we use here all pairs of galaxies, the signal-to-noise of the large-angle dipole will be even larger that the one plotted in figure 12. Note that this dipole could provide an alternative way of measuring redshift-space distortions than the quadrupole.

Finally, let us mention the following point: from eq. (35) it seems that by combining the measurements of the monopole, the quadrupole and the large-angle dipole, we can directly measure the comoving distance r

$$r = \frac{d}{\langle\hat{\xi}^{\rm large}\rangle}\left[\zeta_0(d) - \frac{1}{5}\zeta_2(d)\right]\,. \quad (38)$$

However the distance measured in this way is not the true distance but rather the distance in the fiducial cosmology used to measure the multipoles. The relation between the dipole, the monopole and the quadrupole is indeed due to the fact that in the full sky $\cos\beta_{\rm AB}$ and $\cos\beta_{\rm BA}$ are related through eq. (14). This relation is a geometrical relation which is valid in *any* fiducial cosmology. Therefore contrary to the position of the BAO peak, this relation does not allow us to test the validity of the fiducial cosmology. Note however that we can use the dipole to measure the position of the BAO peak, in a similar way as is done with the monopole, see figures 11 and 17.

4 CONCLUSIONS

We present for the first time a measurement of the dipole in the cross-correlation function of bright and faint galaxies in the LOWz and CMASS samples of the BOSS survey. We show that the dipole depends strongly on the choice of kernel used to measure it. In particular, using the median angle $\mu_{12} = \cos\sigma$, we find that the dipole is given by the sum of relativistic distortions, evolution effects and wide-angle effects. Applying our method to the LOWz and CMASS samples, we show that this dipole is too small to be detected since its signal-to-noise is of the order of 0.2. On

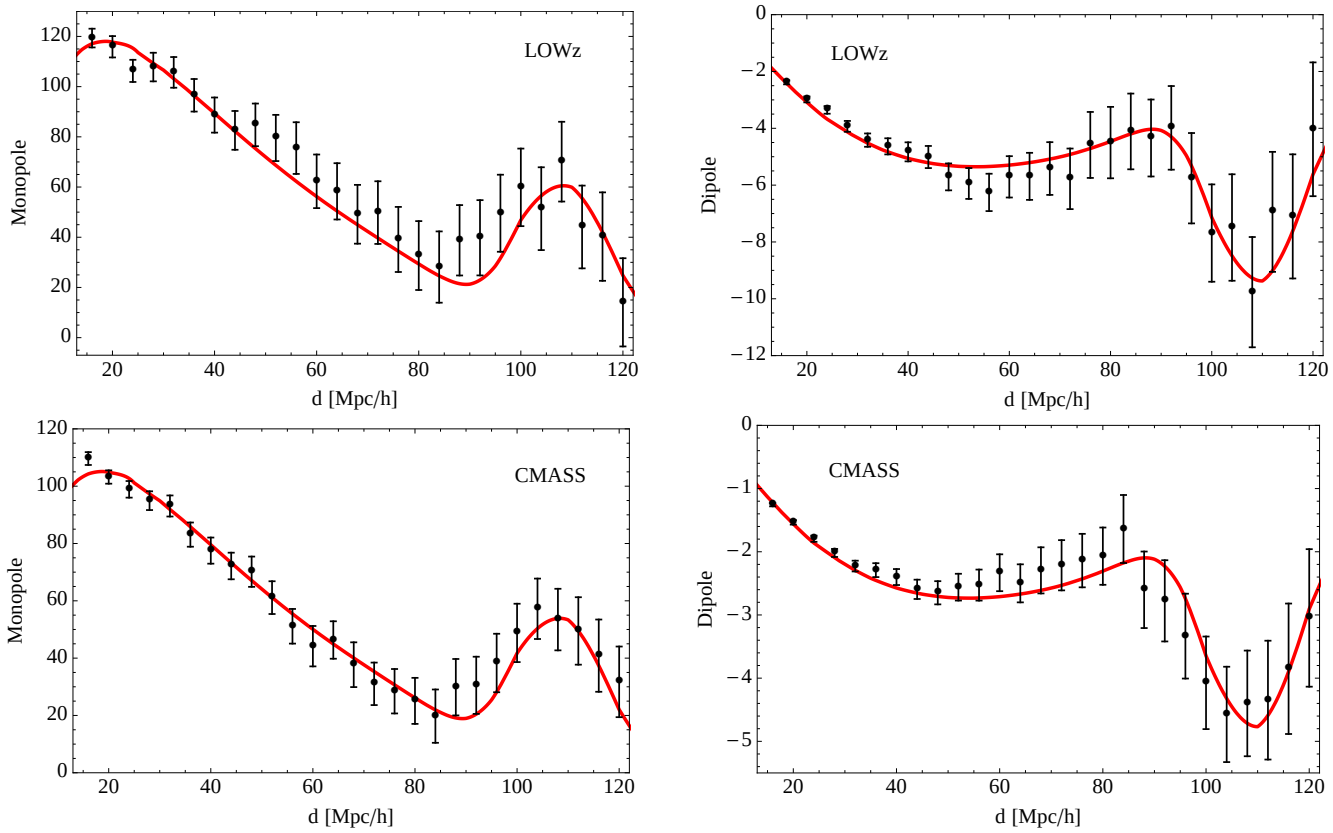

Figure 17. Measurements of the monopole and dipole with one population of galaxies, using the difference of angles $\mu_1 - \mu_{12} = \cos\beta - \cos\sigma$, multiplied by d^2 and plotted as a function of separation. The red solid line is the prediction using linear perturbation theory and the bias is fitted from the monopole.

the other hand, we show that by using the angle difference $\mu_1 - \mu_{12} = \cos\beta - \cos\sigma$ we generate a large-angle dipole, while simultaneously reducing the error by a factor d/r. As a consequence we are able to robustly measure this large-angle dipole using this kernel, with a signal-to-noise of 50.

The wide-angle effect has already been discussed in detail in various works (see e.g. Hamilton 1997; Szalay et al. 1998; Szapudi 2004; Papai & Szapudi 2008; Raccanelli et al. 2010; Samushia et al. 2012; Montanari & Durrer 2012; Bertacca et al. 2012; Yoo & Seljak 2015; Reimberg et al. 2015). In particular, these papers showed that this effect has to be consistently included in the predictions in order to correctly interpret the measurements of the monopole, quadrupole and hexadecapole at large scales. Here we make a distinction between the wide-angle effect and the large-angle effect. We call wide-angle effect the intrinsic wide-angle contribution generated by the fact that redshift-space distortions depend on the two line-of-sights to the galaxies, and not only on one line-of-sight as assumed in the distant-observer (also called the plane-parallel) approximation. Besides this intrinsic wide-angle effect, we show that depending on the choice of kernel we can generate other large-scale contributions, suppressed by one or more powers of d/r. We call these additional geometrical contributions the large-angle effect.

We show a measurement of the large-angle effect in BOSS. The reasons why the large-angle effect is detectable in the dipole whereas it is subdominant in the even multipoles (i.e. monopole, quadrupole and hexadecapole) are the followings. First, just by symmetry the dipole allows to isolate the large-angle effect because it measures the difference between line-of-sight forward and backward directions. In the even multipoles on the other hand the large-angle effect is averaged out as there is no distinction between forward and backward directions: the large-angle effect is therefore a subdominant correction to the flat-sky expression. Second, the large-angle contribution to the dipole is of the order of d/r, whereas the large-angle contribution to even multipoles is of the order of $(d/r)^2$, i.e. significantly smaller (see Bonvin et al. 2014; Reimberg et al. 2015). Finally the error on the dipole is of the order of d/r, i.e. of the same order of magnitude as the signal itself, whereas the error on the even multipoles is of the order of $(d/r)^0$. These three reasons explain why a robust detection of the large-angle effect in the dipole is possible at intermediate scales, probed by the BOSS survey.

We emphasise that the large-angle dipole *does not* contain any new statistical information, since it is just a geometrical combination of the monopole and the quadrupole. However it is conceivable that this dipole is sensitive to different systematics than the monopole and the quadrupole. For example since the kernel to isolate the dipole is anti-symmetric, all types of systematics which are symmetric will automatically cancel out from the dipole. The large-angle dipole could therefore be used as an alternative to the quadrupole to measure redshift-space distortions.

Our analysis shows that the relativistic distortions, which include the effect of gravitational redshift, are not detectable in the BOSS survey. Comparing our predictions with the measurement of gravitational redshift in clusters, we find that the signal in BOSS is 10 times smaller. This difference is likely due to the fact that in clusters one has additional information– the boundaries of the clusters– which can be used to measure the gravitational redshift effect.

This however does not mean that the relativistic effects cannot be detected at all in large-scale structure. The BOSS survey turns out not to be the optimal survey to measure the relativistic dipole. First the mean redshift of the survey is relatively high ($\bar{z} = 0.303$ for LOWz and $\bar{z} = 0.575$ for CMASS). The relativistic distortions decrease quickly with redshift, meaning that a survey at lower redshift may be more appropriate. Second, BOSS selects Luminous Red Galaxies (LRG), which are quite similar in terms of bias. A survey with more diverse types of galaxies would therefore be better to measure the relativistic dipole. Finally, in our analysis we split the survey into two populations only. As a consequence all the correlations within the bright population and within the faint population are lost. A more clever splitting may increase the signal-to-noise of the dipole. In a companion paper (Bonvin et al. 2015), we show how to construct an optimal estimator to measure the relativistic dipole with an arbitrary number of galaxies' populations. We predict that in the main sample of the SDSS data release DR5, using 6 populations, the cumulative signal-to-noise of the relativistic dipole reaches 2.4. With the up-comming DESI (Dark Energy Spectroscopic Instrument) Bright Galaxy Survey (Cahn et al. 2015) which will contain significantly more galaxies than SDSS we predict a cumulative signal-to-noise of 7.4 for the relativistic dipole, showing that a clear detection of gravitational redshift in large-scale structure should be possible in the near future.

Acknowledgments: It is a pleasure to thank Rupert Croft, Alex Hall, Ofer Lahav and Francesco Montanari for interesting and useful discussions. EG acknowledges support from projects AYA2012-39559 and Consolider-Ingenio CSD2007-00060 from he Spanish Ministerio de Ciencia e Innovacion (MICINN) and CosmoComp (PITNGA-2009-238356) and LACEGAL (PIRSES-GA-2010-269264) from the European Commission. LH is support in part by the DOE and NASA.

APPENDIX A: OTHER CHOICE OF KERNEL

In Bonvin et al. (2015) we use a slightly different choice of kernel than in eq. (4). Instead of defining the angle $\cos\gamma_{ij L_i L_j}$ with respect to the bright galaxy in the pair, as done in (5), we define it with respect to the first pixel in the pair, i.e. i. We then multiply the pair of pixels by $+1$ if the pixel i is bright and the pixel j is faint, and by -1 if the pixel i is faint and the pixel j is bright. Such a kernel can be written as

$$w_{\mathbf{x}_i\mathbf{x}_j L_i L_j} = a_N \Big[\theta(L_i - L_j) - \theta(L_j - L_i)\Big] \cos\gamma_{ij}\, \delta_K(d_{ij} - d)\,, \tag{A1}$$

where θ is the Heaviside function and a_N is defined in eq. (6).

The relativistic dipole and the evolution dipole are exactly the same with this choice of kernel. They are given by eqs. (7) and (8). The wide angle dipole is given by

$$\langle\hat{\xi}^{\mathrm{wide}\,2\,\sigma}\rangle = a_N d\bar{n}_{\mathrm{B}} d\bar{n}_{\mathrm{F}} \sum_{ij} \cos\sigma_{ij}\, \delta_K(d_{ij} - d) \times \Big[\langle\Delta_{\mathrm{B}}(\mathbf{x}_i)\Delta_{\mathrm{F}}(\mathbf{x}_j)\rangle - \langle\Delta_{\mathrm{B}}(\mathbf{x}_j)\Delta_{\mathrm{F}}(\mathbf{x}_i)\rangle\Big]^{\mathrm{wide}}, \tag{A2}$$

if we use the angle σ and by

$$\langle\hat{\xi}^{\mathrm{wide}\,2\,\beta}\rangle = a_N d\bar{n}_{\mathrm{B}} d\bar{n}_{\mathrm{F}} \sum_{ij} \cos\beta_{ij}\, \delta_K(d_{ij} - d) \times \Big[\langle\Delta_{\mathrm{B}}(\mathbf{x}_i)\Delta_{\mathrm{F}}(\mathbf{x}_j)\rangle - \langle\Delta_{\mathrm{B}}(\mathbf{x}_j)\Delta_{\mathrm{F}}(\mathbf{x}_i)\rangle\Big]^{\mathrm{wide}}, \tag{A3}$$

if we use the angle β (note that this is the case used in Bonvin et al. (2014)). Since the bracket is already of order d_{ij}/r, these two expressions are equivalent and similar to eq. (11). We have therefore

$$\langle\hat{\xi}^{\mathrm{wide}\,2\,\sigma}\rangle = \langle\hat{\xi}^{\mathrm{wide}\,2\,\beta}\rangle = \langle\hat{\xi}^{\mathrm{wide}\,\sigma}\rangle = \frac{2f}{5}(b_{\mathrm{B}} - b_{\mathrm{F}})\frac{d}{r}C_2(d)\,. \tag{A4}$$

To summarise, we have 4 possible choices of kernel. We have two different possibilities of choosing the angle and two different possibilities of choosing the dependence in luminosity. Three of these possibilities give exactly the same wide-angle contribution (A4). The other possibility, which consists in choosing kernel (4) with the angle β, gives an additional contribution, the large-angle dipole, calculated in eq. (16).

APPENDIX B: EXPLICIT CALCULATION OF THE WIDE-ANGLE EFFECT IN TERMS OF THE ANGLE σ

In Bonvin et al. (2014) we derived a general expression, valid in the full sky, for the standard part of the two-point correlation function

$$\langle\Delta_{\mathrm{B}}(\mathbf{x}_i)\Delta_{\mathrm{F}}(\mathbf{x}_j)\rangle = \frac{2A}{9\pi^2\Omega_m^2}\Big\{S_1 + S_2\cos(2\beta_{ij}) + S_3\cos(2\alpha_{ij}) + S_4\cos(2\alpha_{ij})\cos(2\beta_{ij}) + S_5\sin(2\alpha_{ij})\sin(2\beta_{ij})\Big\}, \tag{B1}$$

where A is the primordial amplitude of perturbations, S_α are coefficients defined in appendix C of Bonvin et al. (2014) [8] and $\alpha_{ij} = \beta_{ji} - \pi$. We want to rewrite β_{ij} and α_{ij} as a function of σ_{ij}. From figure 1 we have

$$\cos(2\beta_{ij}) = \cos(2\sigma_{ij}) - \frac{d_{ij}}{r}\sin(2\sigma_{ij})\sin(\sigma_{ij}) + \mathcal{O}\left(\frac{d_{ij}}{r}\right)^2,$$
$$\cos(2\alpha_{ij}) = \cos(2\sigma_{ij}) + \frac{d_{ij}}{r}\sin(2\sigma_{ij})\sin(\sigma_{ij}) + \mathcal{O}\left(\frac{d_{ij}}{r}\right)^2,$$
$$\sin(2\alpha_{ij})\sin(2\beta_{ij}) = \sin^2(2\sigma_{ij}) + \mathcal{O}\left(\frac{d_{ij}}{r}\right)^2. \tag{B2}$$

[8] The coefficients S_2 and S_3 in Bonvin et al. (2014) have a typo: there should be a minus sign in front of 1/28.

With this we obtain up to order d_{ij}/r

$$\langle \Delta_{\rm B}(\mathbf{x}_i)\Delta_{\rm F}(\mathbf{x}_j)\rangle = \frac{2A}{9\pi^2\Omega_m^2}\Big\{S_1 + S_2\Big[\cos(2\sigma_{ij}) - \frac{d_{ij}}{r}\sin(2\sigma_{ij})\sin(\sigma_{ij})\Big] + S_3\Big[\cos(2\sigma_{ij}) + \frac{d_{ij}}{r}\sin(2\sigma_{ij})\sin(\sigma_{ij})\Big] + S_4\cos^2(2\sigma_{ij}) + S_5\sin^2(2\sigma_{ij})\Big\}. \quad \text{(B3)}$$

The dipole part of eq. (B3) is given by

$$\langle \Delta_{\rm B}(\mathbf{x}_i)\Delta_{\rm F}(\mathbf{x}_j)\rangle^{\rm dip} = \frac{2A}{9\pi^2\Omega_m^2}\frac{4}{5}(S_3 - S_2)\frac{d_{ij}}{r}\cos\sigma_{ij}\,. \quad \text{(B4)}$$

As already noted in Reimberg et al. (2015), in the case of one population of galaxies $S_2 = S_3$ and there is no wide-angle contribution to the dipole with this choice of angle. On the other hand, with two populations of galaxies we find

$$\langle \Delta_{\rm B}(\mathbf{x}_i)\Delta_{\rm F}(\mathbf{x}_j)\rangle^{\rm dip} = -\frac{2f}{5}(b_{\rm B} - b_{\rm F})\frac{d_{ij}}{r}C_2(d_{ij})\cos\sigma_{ij} \quad \text{(B5)}$$

$$= -\langle \Delta_{\rm F}(\mathbf{x}_i)\Delta_{\rm B}(\mathbf{x}_j)\rangle^{\rm dip}\,. \quad \text{(B6)}$$

Inserting this into eq. (11) we obtain eq. (12).

REFERENCES

Anderson L., et al., 2014, Mon. Not. Roy. Astron. Soc., 441, 24
Bertacca D., Maartens R., Raccanelli A., Clarkson C., 2012, JCAP, 1210, 025
Bonvin C., 2014, Class. Quant. Grav., 31, 234002
Bonvin C., Durrer R., 2011, Phys. Rev., D84, 063505
Bonvin C., Hui L., Gaztanaga E., 2014, Phys. Rev., D89, 083535
Bonvin C., Hui L., Gaztanaga E., 2015, in preparation
Cabre A., Gaztanaga E., 2009, Mon. Not. Roy. Astron. Soc., 393, 1183
Cabre A., Gaztanaga E., 2011, Mon. Not. Roy. Astron. Soc., 412, 98
Cahn R. N., Bailey S. J., Dawson K. S., Forero Romero J., Schlegel D. J., White M., DESI 2015, in American Astronomical Society Meeting Abstracts. p. 336.10
Challinor A., Lewis A., 2011, Phys. Rev., D84, 043516
Croft R. A. C., 2013, Mon. Not. Roy. Astron. Soc., 434, 3008
Dai L., Kamionkowski M., Kovetz E. D., Raccanelli A., Shiraishi M., 2015
Di Dio E., Montanari F., Durrer R., Lesgourgues J., 2014, JCAP, 1401, 042
Gaztanaga E., Cabre A., Hui L., 2009, Mon. Not. Roy. Astron. Soc., 399, 1663
Guzzo L., et al., 2008, Nature, 451, 541
Hamilton A. J. S., 1992, ApJ, 385, L5
Hamilton A. J. S., 1997, in Ringberg Workshop on Large Scale Structure Ringberg, Germany, September 23-28, 1996. (arXiv:astro-ph/9708102), http://alice.cern.ch/format/showfull?sysnb=0255366
Hawkins E., et al., 2003, Mon. Not. Roy. Astron. Soc., 346, 78
Jeong D., Schmidt F., Hirata C. M., 2012, Phys. Rev., D85, 023504
Kaiser N., 1987, Mon. Not. Roy. Astron. Soc., 227, 1
Kaiser N., 2013, Mon. Not. Roy. Astron. Soc., 435, 1278
Kogut A., et al., 1993, Astrophys. J., 419, 1
Lilje P. B., Efstathiou G., 1989, MNRAS, 236, 851
McDonald P., 2009, JCAP, 0911, 026
Montanari F., Durrer R., 2012, Phys. Rev., D86, 063503
Papai P., Szapudi I., 2008, Mon. Not. Roy. Astron. Soc., 389, 292
Raccanelli A., Samushia L., Percival W. J., 2010, Mon. Not. Roy. Astron. Soc., 409, 1525
Raccanelli A., Bertacca D., Doré O., Maartens R., 2014, JCAP, 1408, 022
Reimberg P. H. F., Bernardeau F., Pitrou C., 2015
Sadeh I., Feng L. L., Lahav O., 2015, Phys. Rev. Lett., 114, 071103
Samushia L., Percival W. J., Raccanelli A., 2012, Mon. Not. Roy. Astron. Soc., 420, 2102
Samushia L., et al., 2014, Mon. Not. Roy. Astron. Soc., 439, 3504
Song Y.-S., Sabiu C. G., Kayo I., Nichol R. C., 2011, JCAP, 1105, 020
Szalay A. S., Matsubara T., Landy S. D., 1998, Astrophys. J., 498, L1
Szapudi I., 2004, Astrophys. J., 614, 51
Wojtak R., Hansen S. H., Hjorth J., 2011, Nature, 477, 567
Yoo J., 2010, Phys. Rev., D82, 083508
Yoo J., Seljak U., 2015, Mon. Not. Roy. Astron. Soc., 447, 1789
Yoo J., Fitzpatrick A. L., Zaldarriaga M., 2009, Phys. Rev., D80, 083514
Yoo J., Hamaus N., Seljak U., Zaldarriaga M., 2012, Phys. Rev., D86, 063514
Zehavi I., et al., 2005, Astrophys. J., 621, 22
Zhao H., Peacock J. A., Li B., 2013, Phys. Rev. D, 88, 043013

This paper has been typeset from a TEX/LATEX file prepared by the author.